Chaos

Clustering and Bellerophon state in Kuramoto model with second-order coupling

Cite as: Chaos **29**, 043102 (2019); https://doi.org/10.1063/1.5085407
Submitted: 12 December 2018 . Accepted: 11 March 2019 . Published Online: 03 April 2019

Xue Li, Jiameng Zhang, Yong Zou, and Shuguang Guan

Clustering and Bellerophon state in Kuramoto model with second-order coupling

Cite as: Chaos **29**, 043102 (2019); doi: 10.1063/1.5085407
Submitted: 12 December 2018 · Accepted: 11 March 2019 ·
Published Online: 3 April 2019

View Online Export Citation CrossMark

Xue Li, Jiameng Zhang, Yong Zou, and Shuguang Guan[a)]

AFFILIATIONS

Department of Physics, East China Normal University, Shanghai 200241, China

[a)]**Author to whom correspondence should be addressed:** guanshuguang@hotmail.com

ABSTRACT

In this paper, clustering in the Kuramoto model with second-order coupling is investigated under the bimodal Lorentzian frequency distribution. By linear stability analysis and the Ott-Antonsen ansatz treatment, the critical coupling strength for the synchronization transition is obtained. The theoretical results are further verified by numerical simulations. It has been revealed that various synchronization paths, including the first- and second-order transitions as well as the multiple bifurcations, exist in this system with different parameters of frequency distribution. In certain parameter regimes, the Bellerophon states are observed and their dynamical features are fully characterized.

For more than four decades, extensive researches on synchronization have been carried out based on the Kuramoto-like models, in which simple phase oscillators are coupled via the mean-field. So far, most works in this field focused on the situation where the phase oscillators are coupled through the sine function, i.e., the first-order harmonics. Recently, attention has been paid to the case of higher-order coupling, especially the second-order coupling. On the other hand, one important issue in the study of synchronization in coupled phase oscillators is how the distribution of natural frequencies of oscillators affect the system's collective behavior. Typically, two types of frequency distributions are frequently considered, namely, the unimodal and bimodal distributions. In the present work, we investigate the clustering synchronization of the Kuramoto model with second-order coupling under the bimodal Lorentzian frequency distribution. By both theoretical analysis and numerical simulations, significant results have been obtained, which will provide us a better understanding of synchronization of coupled oscillators.

I. INTRODUCTION

Synchronization refers to coherent rhythm in a dynamical system which consists of interacting elements. Typical examples include the circadian rhythms of plants and animals,[1] the synchronized flashing of fireflies,[2] the Josephson junction arrays,[3] and neurons in the human brain,[4] just to name a few. It is now understood that the emergence of coherence is crucial for the cooperative functioning in many dynamical systems. Due to this reason, such phenomena have been extensively investigated in various fields. A comprehensive review of synchronization can be found in Ref. 5.

One prototype model for the theoretical study on synchronization is the Kuramoto model,[6,7] which describes the synchronization transition among phase oscillators via mean-field coupling. Although it has been studied for over 40 years, recently the research studies on certain generalized Kuramoto models have presented novel physics, such as the explosive (i.e., the first-order) synchronization,[8–10] the Chimera states,[11,12] and the Bellerophon (B) states.[13,14]

The general form of the Kuramoto-like equation can be expressed as

$$\dot{\theta}_i = \omega_i + \frac{\kappa}{N}\sum_{j=1}^{N} H(\theta_j - \theta_i), \quad i = 1, 2, \ldots, N, \tag{1}$$

where θ_i and ω_i are the phase and the natural frequency of the ith oscillator and the dot denotes the time derivative. The second term of the right-hand side is the coupling, where H is a 2π-periodic function. If it takes the first-order term of H in a Fourier expansion, i.e., $H(\theta) = \sin\theta$, Eq. (1) recovers the standard Kuramoto model,

$$\dot{\theta}_i = \omega_i + \frac{\kappa}{N}\sum_{j=1}^{N} \sin(\theta_j - \theta_i), \quad i = 1, 2, \ldots, N. \tag{2}$$

This model and its variants have been extensively studied. In fact, H could also take higher harmonic terms of the Fourier expansion. For example, Refs. 15–19 have studied the Kuramoto model with the following bi-harmonic coupling terms, where $H(\theta) = \sin\theta + \sin 2\theta$, i.e., including both the first- and second-order harmonics. Recently, Ref. 20 investigated the case where phase oscillators are coupled only with the second-order harmonic term, i.e.,

$$\dot{\theta}_i = \omega_i + \frac{\kappa}{N}\sum_{j=1}^{N}\sin\left[2(\theta_j - \theta_i)\right], \quad i = 1, 2, \ldots, N. \tag{3}$$

It should be pointed out that, although Eqs. (3) and (2) look similar in form, they are not equivalent since Eq. (3) cannot be recovered into Eq. (2) by a linear transformation of phase. Interestingly, in such a case, oscillators turn out to form two coherent clusters, with phase difference π. This means that the π-state, rather than the single-cluster synchronized state, is the stable manifold of synchronization in this system. In Ref. 21, the synchronization induced by the finite size effect was investigated in the Kuramoto model with a purely nonlinear second-harmonic coupling. We notice that in previous studies, the natural frequencies ω_i are typically drawn from the unimodal distributions, such as the Lorentzian distribution[20] or the Gaussian distribution.[21] Motivated by these works, in this paper, we will focus on another important frequency distribution, i.e., the bimodal Lorentzian distribution

$$g(\omega) = \frac{\Delta}{2\pi}\left(\frac{1}{(\omega-\omega_0)^2+\Delta^2} + \frac{1}{(\omega+\omega_0)^2+\Delta^2}\right), \tag{4}$$

where 2Δ is the width at half-maximum of each peak and $\pm\omega_0$ are the center frequencies of two peaks. Notice that when $\Delta > \sqrt{3}\omega_0$, the bimodal distribution becomes the unimodal one.

In this work, we present two types of theoretical analyses to Eq. (3) with distribution Eq. (4). In Sec. II, we apply linear stability analysis to the incoherent state and obtain the critical coupling strength for the transition of clustering synchronization. Then, in Sec. III, an analysis based on the Ott-Antonsen (OA) ansatz is performed and once again, the critical point for synchronization is solved. In Sec. IV, the theoretical results are further verified by numerical simulations. Besides the usual π-state, we found that the Bellerophon states could occur in this model. The specific dynamical features of the Bellerophon states are characterized in detail. Finally, the main conclusion will be drawn in Sec. V.

II. LINEAR STABILITY ANALYSIS

As pointed in Ref. 20, under certain circumstances, the second-order coupling Kuramoto model might exhibit some clustering behaviors that generally lack in the standard Kuramoto model. To characterize the level of clustering coherence of phase oscillators governed by Eq. (3), two order parameters

$$r_m e^{im\psi_m} = \frac{1}{N}\sum_{j=1}^{N} e^{im\theta_j}, \quad m = 1, 2 \tag{5}$$

can be defined.[20] In principle, both r_1 and r_2 should be used to fully characterize the higher order coherence in system (3).[20] The state with $r_m = 0$, for all m corresponds to a totally incoherent state where the phases of oscillators are uniformly distributed, while non-zero values of at least one order parameter indicate for certain synchrony in the ensemble of oscillators. In model (3), the oscillators tend to form two clusters due to the second-order coupling. Therefore, in this system, order parameter r_2 describes the degree of two-cluster synchrony, while r_1 measures the degree of asymmetry in such clustering (or the global synchronization trend).[20]

By introducing order parameter r_2, Eq. (3) can be rewritten as the following mean-field form:

$$\dot{\theta}_i = \omega_i + \kappa r_2 \sin(2\psi_2 - 2\theta_i), \quad i = 1, 2, \ldots, N. \tag{6}$$

Based on this mean-form equation, we can apply theoretical analysis on the transition of clustering synchronization characterized by order parameter r_2. To characterize the global synchronization, we numerically compute the order parameter r_1. We consider the thermodynamical limit, i.e., $N \to \infty$. In this case, a continuum description can be obtained by introducing the density function $f(\theta, \omega, t)$, which describes the density of oscillators with phase θ and natural frequency ω at time t. The evolution of $f(\theta, \omega, t)$ is governed by the continuity equation

$$\frac{\partial f}{\partial t} + \frac{\partial (f\dot{\theta})}{\partial \theta} = 0. \tag{7}$$

Then, a linear stability analysis can be achieved based on the mean-field equation and the continuity equation. Following the standard procedure as in Refs. 7 and 9, we obtain the characteristic equation which relates explicitly the coupling strength κ with the eigenvalue λ, i.e.,

$$1 = \kappa\int_{-\infty}^{+\infty}\frac{g(\omega)}{\lambda + 2i\omega}\,d\omega. \tag{8}$$

The real part of λ determines the stability of the incoherent state, i.e., when $\mathrm{Re}(\lambda)$ changes from negative to positive, the incoherent state loses its stability. One can then use this condition to determine the critical coupling strength κ_f for the forward synchronization transition. Substituting Eq. (4) into the above equation, we get

$$\frac{1}{\kappa} = \int_{-\infty}^{+\infty}\left[f_1(\omega) + f_2(\omega)\right]\,d\omega, \tag{9}$$

where

$$f_1(\omega) = \frac{1}{\lambda + 2i\omega}\,\frac{\Delta}{2\pi}\,\frac{1}{(\omega-\omega_0)^2+\Delta^2}, \tag{10}$$

$$f_2(\omega) = \frac{1}{\lambda + 2i\omega}\,\frac{\Delta}{2\pi}\,\frac{1}{(\omega+\omega_0)^2+\Delta^2}. \tag{11}$$

For generalized Kuramoto models, there is no guarantee that λ in Eq. (8) is necessarily real. Thus, one has to consider the general situation assuming λ is complex as $\lambda = a + ib$ ($a, b \in \mathbb{R}$, and $b \neq 0$). In the following, we discuss three distinct cases, corresponding to $a > 0$, $a = 0$, and $a < 0$, respectively. Note that we can apply analytic continuation for $g(\omega)$ to the whole complex plane. So the integral in Eq. (9) can be conveniently done by choosing a contour either in the lower half complex plane or in the upper complex plane.

1. $a > 0$. In this case, in the lower half complex plane, f_1 has one pole $\omega_0 - i\Delta$, while f_2 has another one $-\omega_0 - i\Delta$. Equation (9)

becomes

$$\frac{1}{\kappa} = -2\pi i \left[\mathrm{Res}(\omega_0 - i\Delta, f_1) + \mathrm{Res}(-\omega_0 - i\Delta, f_2)\right]$$
$$= \frac{\lambda + 2\Delta}{(\lambda + 2\Delta)^2 + 4\omega_0^2}, \tag{12}$$

where Res means the residue. From this equation, we can explicitly get the closed form of the eigenvalue as

$$\lambda = \frac{\kappa \pm \sqrt{\kappa^2 - 16\omega_0^2}}{2} - 2\Delta. \tag{13}$$

Notice that $a > 0$ is assumed from the beginning, and we can use the condition $\mathrm{Re}[\lambda] \to 0^+$ to determine the critical coupling strength for the synchronization transition, which leads to

$$\kappa_f = \begin{cases} 4\Delta & (\Delta \le \omega_0), \\ 2(\Delta^2 + \omega_0^2)/\Delta & (\Delta > \omega_0). \end{cases} \tag{14}$$

2. $a = 0$. In this case, the eigenvalue $\lambda = ib$. $f_1(\omega)$ has one pole $-b/2$ in the real axis and one pole $\omega_0 + i\Delta$ in the upper half plane. In the mean time, $f_2(\omega)$ has one pole $-b/2$ in the real axis and one pole $-\omega_0 + i\Delta$ in the upper half plane. Therefore, Eq. (9) becomes

$$\frac{1}{\kappa} = 2\pi i \mathrm{Res}(\omega_0 + i\Delta, f_1) + \pi i \mathrm{Res}\left(-\frac{b}{2}, f_1\right)$$
$$+ 2\pi i \mathrm{Res}(-\omega_0 + i\Delta, f_2) + \pi i \mathrm{Res}\left(-\frac{b}{2}, f_2\right)$$
$$= 0 + i\frac{\frac{b}{4}(-b^2 - 4\Delta^2 + 4\omega_0^2)}{4[(\frac{b}{2} + \omega_0)^2 + \Delta^2][(-\frac{b}{2} + \omega_0)^2 + \Delta^2]}. \tag{15}$$

According to the above equation, obviously, κ is purely complex regardless of Δ and ω_0. So this case is not physical and should be neglected. By the way, from Eq. (15) the eigenvalue can also be explicitly solved as

$$\lambda = 2\sqrt{\omega_0^2 - \Delta^2}\, i \quad (\Delta \le \omega_0), \tag{16}$$

which is a purely imaginary number, consistent with the assumption $a = 0$ in the start.

3. $a < 0$. In this case, $f_1(\omega)$ has one pole $\omega_0 + i\Delta$ in the upper half plane, while $f_2(\omega)$ has one pole $-\omega_0 + i\Delta$ in the upper half plane. Therefore, Eq. (9) can be written as

$$\frac{1}{\kappa} = 2\pi i \left[\mathrm{Res}(\omega_0 + i\Delta, f_1) + \mathrm{Res}(-\omega_0 + i\Delta, f_2)\right]$$
$$= \frac{\lambda - 2\Delta}{(\lambda - 2\Delta)^2 + 4\omega_0^2}. \tag{17}$$

From this equation, the eigenvalue can be analytically obtained as

$$\Longrightarrow \lambda = \frac{\kappa \pm \sqrt{\kappa^2 - 16\omega_0^2}}{2} + 2\Delta. \tag{18}$$

Notice that, as $a < 0$ has been assumed, one can determine the critical coupling strength by setting $\mathrm{Re}[\lambda] \to 0^-$, i.e.,

$$\kappa_f = \begin{cases} -4\Delta & (\kappa < 4\omega_0), \\ -2(\Delta^2 + \omega_0^2)/\Delta & (\kappa \ge 4\omega_0). \end{cases} \tag{19}$$

Since Δ characterizes the width of the peaks in the frequency distribution, physically, we always have $\Delta > 0$. Thus, the above solutions for the critical point are not significant and should be neglected.

To summarize, by linear stability analysis, we have successfully obtained the critical point for the forward transition, i.e., Eq. (14).

III. OA ANALYSIS

In the seminal works,[22,23] Ott and Antonsen proposed a general framework to effectively reduce the dimension of coupled oscillators system. Following Ref. 20, we can use a variation of the OA ansatz to seek a low-dimensional analytical solution for the dynamics of the symmetric part of $f(\theta, \omega, t)$. Specifically, for the symmetric part of $f(\theta, \omega, t)$, it can be expanded as Fourier series

$$f_s(\theta, \omega, t) = \frac{g(\omega)}{2\pi}\left[1 + \sum_{n=1}^{\infty}(f_{2n}(\omega, t)e^{2in\theta} + c.c.)\right], \tag{20}$$

where *c.c.* denotes the complex conjugate of the previous term. For dynamical system (3), the following variation of the OA ansatz on the symmetric part of $f_s(\theta, \omega, t)$ can be used

$$f_{2n}(\omega, t) = \alpha^n(\omega, t). \tag{21}$$

Then, from Eqs. (6), (7), and (21), one can obtain the following ODE for α:

$$\frac{\partial \alpha}{\partial t} + \kappa(r_2\alpha^2 - r_2^*) + 2i\omega\alpha = 0. \tag{22}$$

In the continuum limit, we get

$$r_2(t) = \int_{-\infty}^{\infty}\int_0^{2\pi} e^{2i\theta} f(\theta, \omega, t)\, d\theta\, d\omega$$
$$= \int_{-\infty}^{\infty} g(\omega)\alpha^*(\omega, t)\, d\omega. \tag{23}$$

Substituting the bimodal frequency distribution, i.e., Eq. (4), into the above equation and applying a contour integration in the lower half complex plane, we have

$$r_2(t) = \int_{-\infty}^{\infty} \frac{\Delta}{2\pi}\left(\frac{\alpha^*(\omega, t)}{(\omega - \omega_0)^2 + \Delta^2} + \frac{\alpha^*(\omega, t)}{(\omega + \omega_0)^2 + \Delta^2}\right) d\omega$$
$$= \frac{1}{2}[\alpha^*(-\omega_0 - i\Delta, t) + \alpha^*(\omega_0 - i\Delta, t)]$$
$$= \frac{1}{2}[r_a(t) + r_b(t)], \tag{24}$$

where $r_a(t) = \alpha^*(-\omega_0 - i\Delta, t)$ and $r_b(t) = \alpha^*(\omega_0 - i\Delta, t)$, respectively. Combining Eq. (22) with Eq. (24), one gets

$$\dot{r}_a = -2(\Delta + i\omega_0)r_a + \frac{\kappa}{2}[r_a + r_b - (r_a^* + r_b^*)r_a^2],$$
$$\dot{r}_b = -2(\Delta - i\omega_0)r_b + \frac{\kappa}{2}[r_a + r_b - (r_a^* + r_b^*)r_b^2]. \tag{25}$$

In polar coordinates, we can define

$$r_a = \rho_a e^{i\phi_a}, \quad r_b = \rho_b e^{i\phi_b}, \quad \phi = \phi_b - \phi_a. \tag{26}$$

Then, the 4-ODE system (25) can be reduced into 3 ODEs as

$$\dot{\rho}_a = -2\Delta\rho_a + \frac{\kappa}{2}(1-\rho_a^2)(\rho_a + \rho_b\cos\phi), \tag{27}$$

$$\dot{\rho}_b = -2\Delta\rho_b + \frac{\kappa}{2}(1-\rho_b^2)(\rho_a\cos\phi + \rho_b), \tag{28}$$

$$\dot{\phi} = 4\omega_0 - \frac{\kappa}{2}\frac{\rho_a^2+\rho_b^2+2\rho_a^2\rho_b^2}{\rho_a\rho_b}\sin\phi. \tag{29}$$

Without loss of generality, we now seek for solutions of the above equations that satisfy the symmetry condition

$$\rho_a(t) = \rho_b(t) = \rho(t). \tag{30}$$

As a result, the system can be further simplified into the following 2 ODEs:

$$\dot{\rho} = \frac{\kappa}{2}\rho[1 - \frac{4\Delta}{\kappa} - \rho^2 + (1-\rho^2)\cos\phi], \tag{31}$$

$$\dot{\phi} = 4\omega_0 - \kappa(1+\rho^2)\sin\phi. \tag{32}$$

The incoherent state is defined by $\rho^* = 0$ and $\sin\phi^* = 4\omega_0/\kappa$, which is a fixed point of the 2-dimensional system described by the above ODEs. By linearizing the above equations with respect to this fixed point, we can obtain the characteristic equation as

$$\begin{vmatrix} \left[\frac{\kappa}{2}(1+\cos\phi^*) - 2\Delta\right] - \lambda & 0 \\ 0 & -\kappa\cos\phi^* - \lambda \end{vmatrix} = 0. \tag{33}$$

Noticing that $\cos\phi^* = \pm\sqrt{1-(4\omega_0/\kappa)^2}$, we then obtain Eq. (13), which will lead to the critical point for the forward transition as in Eq. (14). Therefore, the OA analysis gives exactly the same result as the linear stability analysis method does in Sec. II.

IV. NUMERICAL RESULTS

In the above, we have applied both linear stability analysis and OA analysis to obtain the critical point of system (3). On the other hand, we have carried out extensive numerical simulations to investigate the synchronization transitions in this system. In the present work, numerical integrations are performed with a fourth-order Runge-Kutta method with integration time step $\Delta t = 0.01$. The initial conditions for the phase variables are randomly taken and the typical number of oscillators in the ensemble is $N = 10^4$. In the following, we report the numerical results in detail.

In Fig. 1, we compare the critical coupling strength obtained by numerical simulations to the theoretical predictions. The critical coupling strength of the forward transition κ_f is plotted vs Δ for three parameters $\omega_0 = 2.0$, 3.0, and 12.0, respectively. It is shown that the numerical results (circles) fully support the theoretical predictions (solid lines). Specifically, the analytical results, i.e., Eq. (14), predict that the critical point κ_f has two branches of solutions separated by $\Delta \le \omega_0$ and $\Delta > \omega_0$. This feature is totally verified as shown in Fig. 1.

In Fig. 2, we report the rich phenomena of synchronization transitions in dynamical system (3) as the coupling strength varies. We fix parameter $\omega_0 = 2.0$, and let parameter Δ increase. Figure 2(a) plots the order parameter r_2 vs the coupling strength κ for $\Delta = 0.8$.

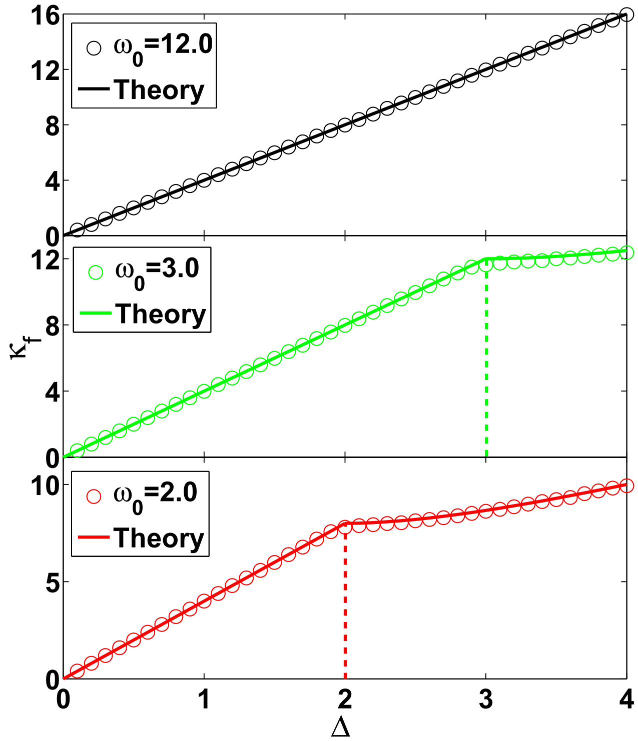

FIG. 1. The critical coupling strength of the forward transition κ_f vs Δ for $\omega_0 =$ 12.0, 3.0, and 2.0, respectively. The numerical results are represented by circles. It is shown that κ_f has two branches of solutions separated by $\Delta = \omega_0$. The numerical results are well consistent with the theoretical predictions (solid lines), i.e., Eq. (14).

In this case, the frequency distribution is a typical bimodal one, as shown in the inset of Fig. 2(a). It is found that the system is in the incoherent state when the coupling strength is small ($\kappa < \kappa_f$). Then, when κ exceeds the critical point, the system bifurcates via a second-order transition into the B state, which is a quantized non-stationary coherent state.[13] As the coupling strength further increases, the system finally achieves the stationary synchronized state. Figure 2(b) describes the synchronization transitions for $\Delta = 1.5$, where the two peaks become a little wider. In this case, the system undergoes two transitions toward synchronization. As the coupling strength exceeds the critical point κ_f, the system first bifurcates via a second-order transition into the B state. Then, further increasing the coupling strength will cause the system to jump into the synchronized state (see the first-order transition in the inset). On the other hand, when the system starts from the synchronized state, as the coupling strength decreases, it will first jump down to the B state via a first-order transition. Then, the system bifurcates into the incoherent state when the coupling strength is smaller than the critical point κ_f. For the second transition, a hysteresis loop is observed which typically characterizes the first-order phase transition. In Fig. 2(c), $\Delta = 1.8$, where the two peaks of frequency distribution become more wider. In this case, two transitions occur in the forward direction. The first one is continuous, where the system bifurcates into

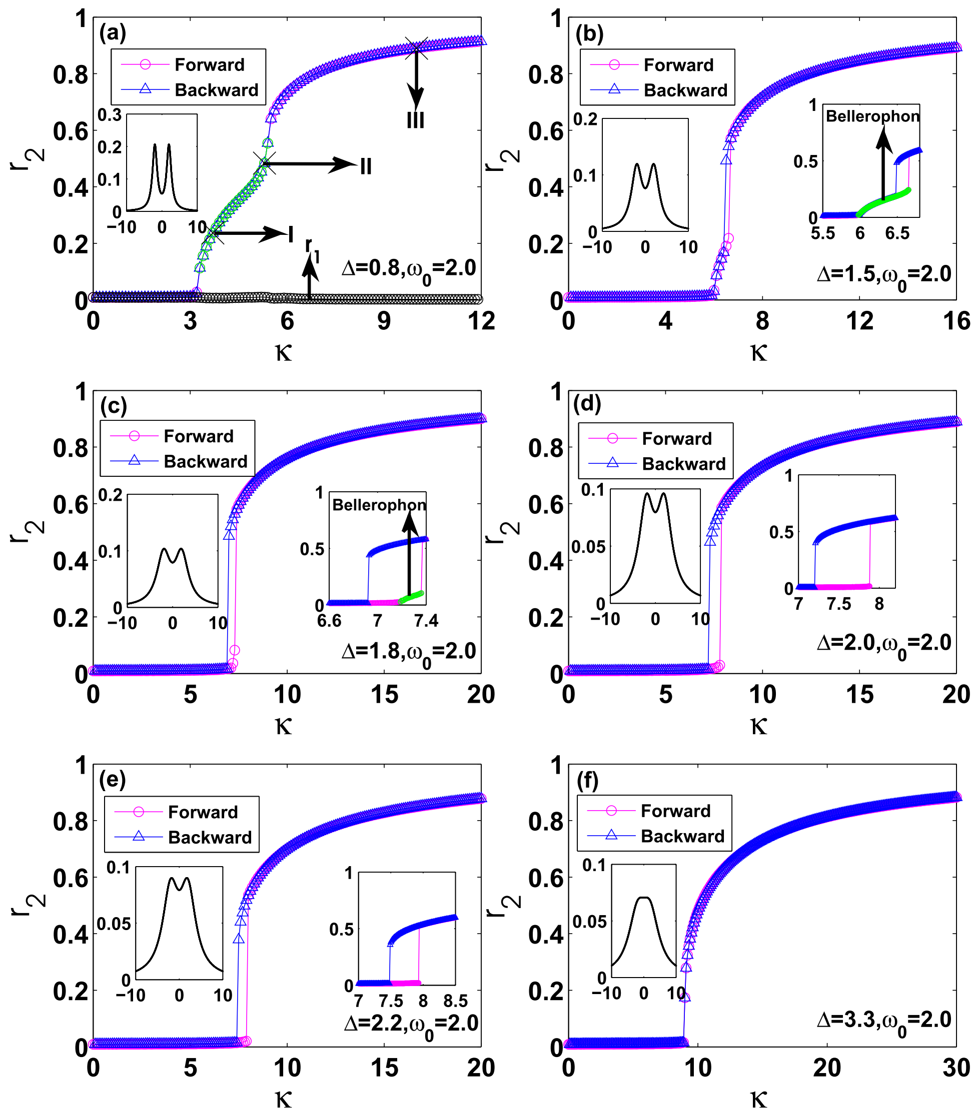

FIG. 2. Typical synchronization transition paths in Eq. (3) with bimodal frequency distribution, characterized by order parameter r_2 vs coupling strength κ. $\omega_0 = 2.0$. The bifurcation scenarios in (a)–(f) correspond to $\Delta = 0.8$, 1.5, 1.8, 2.0, 2.2, and 3.3, respectively, when the two peaks in the distribution become wider and wider. Both forward (pinkish circles) and backward (blue triangles) transitions are numerically studied in an adiabatic way. The regimes of Bellerophon states are denoted by green circles in (a)–(c). The insets show the frequency distributions. In fact, we have also computed r_1 and found they are all 0 in the above six cases. In (a), r_1 is shown as an example (black circles). For better visualization, we do not plot r_1 in the rest panels.

the B state from the initial incoherent state, and the second one is of first-order, where the system jumps from the B state to the final synchronized state. However, this case is different from Fig. 2(b) in the backward direction. When along the backward direction, there is only one first-order transition, where the system directly jumps from the synchronized state back to the incoherent state as shown in the inset of Fig. 2(c). So we observe an interesting synchronization transition path here. There are two successive transitions in the forward direction while only one transition occurs in the backward direction. As parameter Δ increases even larger, which means that the two peaks in the frequency distribution become more and more wider, a typical first-order transition toward synchronization occurs in the system, as shown in Figs. 2(d) and 2(e). In these two cases, B state is not observed in our simulations. The system directly jumps into the synchronized state in the forward direction, and the reverse process happens in the backward transition with a hysteresis loop. As we know, when $\Delta > \sqrt{3}\omega_0$, the bimodal frequency distribution becomes a unimodal one. In Fig. 2(f), we illustrate an example with

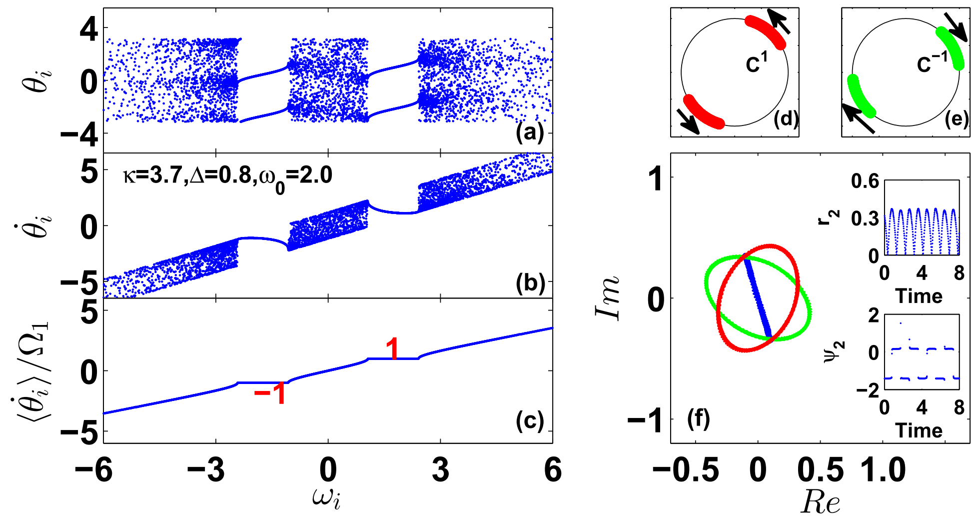

FIG. 3. The B state corresponding to point I in Fig. 2(a). $\kappa = 3.7$. Snapshots of the instantaneous phase θ_i (a), the instantaneous speed $\dot{\theta}_i$ (b), and the average speed $\langle\dot{\theta}_i\rangle$ (c) versus the natural frequencies ω_i of the oscillators. Note that the instantaneous frequencies of oscillators in each coherent cluster are not locked, but their averaged frequencies are locked. Ω_1 is the principle frequency, i.e., the lowest average frequency among coherent clusters. (d) and (e) illustrate the snapshots of coherent oscillators C^1 and C^{-1} on the unit circle. In (f), the local order parameters of the two clusters corresponding to $\omega > 0$ (red) and $\omega < 0$ (green) are plotted, and the global order parameter for all oscillators is the blue line, which oscillates almost periodically as shown by the insets.

$\Delta = 3.3$, which is very close to $\sqrt{3}\omega_0 = 3.46$, i.e., the distribution is approaching a unimodal one as shown in the inset. In this case, there is only one continuous transition toward synchronization as the coupling strength increases. This is just like the situation in the classical Kuramoto model. It should be emphasized that actually, we have also computed order parameter r_1 for the above six cases. It is found that they are typically 0, as illustrated in panel (a) of Fig. 2. These results suggest that although the manifold of global synchronization exists for Eq. (3), it turns out to be unstable for the parameter regimes studied.

We now characterize the typical coherent states observed in the system. In the first example, a B state is illustrated in Fig. 3, which corresponds to point I in Fig. 2(a). In such a state, oscillators with $\omega > 0$ form a π-state, and so do the oscillators with $\omega < 0$, as shown in panels 3(a), 3(d), and 3(e). These two π-states rotate in the opposite direction. However, this is not a standing wave state because the

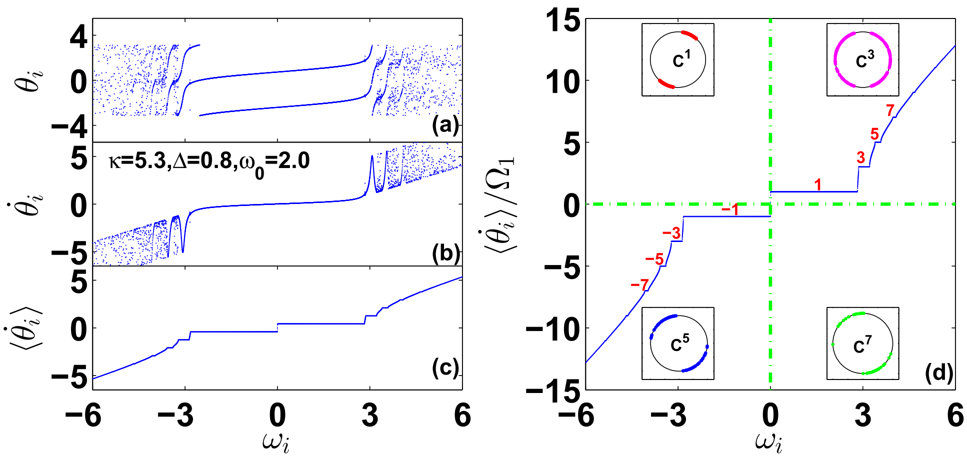

FIG. 4. The B state corresponding to point II in Fig. 2(a) showing multiple symmetric coherent clusters. $\kappa = 5.3$. For (a)–(c), the figure captions are the same as in Fig. 3. (d) Enlargement of the average speeds of the coherent clusters. They correspond to odd-numbered multiples of the principle frequency Ω_1. In the insets, the snapshots for clusters C^1, C^3, C^5, and C^7 are plotted, respectively. Note that all coherent clusters together with the incoherent ones are actually on the same circle.

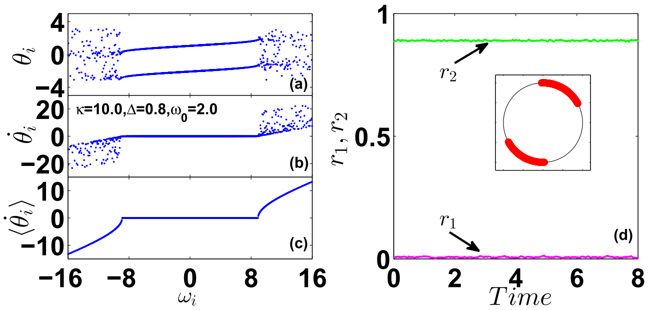

FIG. 5. The π-state corresponding to point III in Fig. 2(a). $\kappa = 10.0$. Contrary to the B states, the instantaneous frequencies of coherent oscillators are locked as shown in (b).

instantaneous frequencies of oscillators in each cluster are not locked [panel 3(b)]. Actually, these are time-dependent. However, it is found that their averaged frequencies are locked [panel 3(c)]. In panel 3(f), the local order parameters for oscillators with $\omega > 0$ (red) and $\omega < 0$ (green) are plotted, which turn out to be two smeared ovals. The global order parameter for all oscillators is the blue line, which oscillates as shown in the insets. So actually this state is a special case of B state, which is non-stationary and has two quantized plateaus in terms of averaged frequencies.

In the second example, a typical B state is shown in Fig. 4, corresponding to point II in Fig. 2(a). In such a state, oscillators split into multiple symmetric coherent clusters [panels 4(a)–4(c)]. The most important characteristic is that the oscillators' instantaneous frequencies are not locked [panel 4(b)], whereas their averaged frequencies form quantized plateaus [panel 4(c)]. In panel 4(d), it is further shown that the staircases of the averaged frequencies correspond to odd-numbered multiples of the principle frequency Ω_1, which is the lowest one. This means that on average the oscillators in cluster $C^{2n-1}, n = 1, 2, 3, \ldots$, rotate $(2n - 1)$ loops, respectively, during the period $2\pi/\Omega_1$. In the insets of panel 4(d), snapshots of oscillators in clusters C^1, C^3, C^5, and C^7 are illustrated. For better visualization, they are plotted on separated circles. Actually, they are all on one circle together with the incoherent drifting oscillators. Therefore, one can imagine a picture of higher-order coherence in this system: oscillators are correlated to a certain extent on the one hand, but still have certain degrees of freedom on the other hand.

Finally, Fig. 5 shows the synchronized state in the system, corresponding to point III in Fig. 2(a). This state is a typical π-state, where oscillators form two coherent clusters. As shown in 5(b), the instantaneous frequencies of oscillators in the coherent clusters are locked. This is essentially different from the B states, as shown in Figs. 3 and 4. In panel 5(d), both order parameters r_1 and r_2 are plotted with respect to time. It is shown that r_2 approaches a value near 1, but r_1 is always approximately zero. This implies that the two clusters in the π-state are symmetric. In fact, since the bimodal Lorentzian distribution is symmetric, we do not observe asymmetric π-state in the current model.

V. CONCLUSION

In this work, we studied synchronization in the Kuramoto model with second-order coupling under the bimodal Lorentzian frequency distribution. By applying theoretical analyses, including both linear stability analysis and the Ott-Antonsen analysis, we have successfully obtained the critical point for synchronization transition. Then, we carried extensive numerical simulations which fully supported the theoretical predictions. Furthermore, it is found that the system has two typical coherent clustering states, i.e., the B state and the π-state, whereas the complete synchronized state has not been observed with such second-order coupling scheme. Finally, various bifurcations among the incoherent state and these two coherent states have been numerically revealed. The present analytical and numerical results will enhance our understandings of collective behavior in coupled oscillator systems.

ACKNOWLEDGMENTS

This work is partially supported by the National Natural Science Foundation of China (Grant Nos. 11875132, 11835003, and 11872182) and the Natural Science Foundation of Shanghai (Grant Nos. 18ZR1411800 and 17ZR1444800).

REFERENCES

[1] A. T. Winfree, "Biological rhythms and the behavior of populations of coupled oscillators," J. Theor. Biol. **16**, 15 (1967).
[2] J. Buck, "Synchronous rhythmic flashing of fireflies. II," Q. Rev. Biol. **63**, 265 (1988).
[3] K. Wiesenfeld, P. Colet, and S. H. Strogatz, "Synchronization transitions in a disordered Josephson series array," Phys. Rev. Lett. **76**, 404 (1996).
[4] G. Buzsáki and A. Draguhn, "Neuronal oscillations in cortical networks," Science **304**, 1926 (2004).
[5] A. Pikovsky, M. Rosenblum, and J. Kurths, *Synchronization: A Universal Concept in Nonlinear Sciences* (Cambridge University Press, Cambridge, 2003).
[6] Y. Kuramoto, *Chemical Oscillations, Waves and Turbulence* (Springer, 1984).
[7] S. H. Strogatz, "From Kuramoto to Crawford: Exploring the onset of synchronization in populations of coupled oscillators," Physica D **143**, 1 (2000).
[8] J. Gómez-Gardeñes, S. Gómez, A. Arenas, and Y. Moreno, "Explosive synchronization transitions in scale-free networks," Phys. Rev. Lett. **106**, 128701 (2011).
[9] X. Hu *et al.* "Exact solution for first-order synchronization transition in a generalized Kuramoto model," Sci. Rep. **4**, 7262 (2014).
[10] S. Boccaletti *et al.* "Explosive transitions in complex networks' structure and dynamics: Percolation and synchronization," Phys. Rep. **660**, 1 (2016).
[11] Y. Kuramoto and D. Battogtokh, "Coexistence of coherence and incoherence in nonlocally coupled phase oscillators," Nonlinear Phenom. Complex Syst. **5**, 380 (2002).
[12] D. M. Abrams and S. H. Strogatz, "Chimera states for coupled oscillators," Phys. Rev. Lett. **93**, 174102 (2004).
[13] H. Bi *et al.* "Coexistence of quantized, time dependent, clusters in globally coupled oscillators," Phys. Rev. Lett. **117**, 204101 (2016).
[14] T. Qiu *et al.* "Synchronization and Bellerophon states in conformist and contrarian oscillators," Sci. Rep. **6**, 36713 (2016).
[15] M. Komarov and A. Pikovsky, "Multiplicity of singular synchronous states in the Kuramoto model of coupled oscillators," Phys. Rev. Lett. **111**, 204101 (2013).
[16] M. Komarov and A. Pikovsky, "The Kuramoto model of coupled oscillators with a bi-harmonic coupling function," Physica D **289**, 18 (2014).
[17] K. Li, S. Ma, H. Li, and J. Yang, "Transition to synchronization in a Kuramoto model with the first- and second-order interaction terms," Phys. Rev. E **89**, 032917 (2014).

[18] H. Wang, W. Han, and J. Yang, "Synchronous dynamics in the Kuramoto model with biharmonic interaction and bimodal frequency distribution," Phys. Rev. E **96**, 022202 (2017).
[19] S. Eydam and M. Wolfrum, "Mode locking in systems of globally coupled phase oscillators," Phys. Rev. E **96**, 052205 (2017).
[20] P. S. Skardal, E. Ott, and J. G. Restrepo, "Cluster synchrony in systems of coupled phase oscillators with higher-order coupling," Phys. Rev. E **84**, 036208 (2011).
[21] M. Komarov and A. Pikovsky, "Finite-size-induced transitions to synchrony in oscillator ensembles with nonlinear global coupling," Phys. Rev. E. **92**, 020901(R) (2015).
[22] E. Ott and T. M. Antonsen, "Low dimensional behavior of large systems of globally coupled oscillators," Chaos **18**, 037113 (2008).
[23] E. Ott and T. M. Antonsen, "Long time evolution of phase oscillator systems," Chaos **19**, 023117 (2009).